Analysis of Radiation Characteristics of Conformal End-Fire Antenna Mounted on a Large Conducting Cylinder

Ping Wang

School of Communications and Information Engineering
Chongqing University of Posts and Telecommunications, Chongqing 400065, China
wangpingcqz@163.com

Abstract ─ An analysis on the effect of dielectric radome on radiation characteristics of conformal end-fire antenna mounted on a large conducting cylinder is presented in this paper. Ray theory firstly is used to characterize the effect of the planar dielectric layer on the incident electromagnetic wave with different polarizations, which predicts the physical behavior of radome-antenna system. Meanwhile, the paper shows a comparing analysis of the effect of dielectric radome on conformal end-fire antenna with different polarization when the antenna is located on the external surface of a hollow conducting cylinder. It is found that the radiation characteristics of end-fire antenna is significantly changed due to the presence of the dielectric radome, and the effect of dielectric radome on vertically polarized end-fire antenna is less than that on horizontally polarized end-fire antenna. Parametric studies of the proposed radome-antenna system are also presented in this paper to explore the interaction mechanism between the endfire antenna and dielectric radome, and provide brief guidelines for the antenna designers. These results may provide some useful insights in the design of the radome-antenna system in practical engineering.

Index Terms ─ Conformal antenna, dielectric radome, end-fire antenna, horizontally polarized antenna, vertically polarized antenna.

I. INTRODUCTION

Dielectric antenna radome consists of single layer or multilayer dielectric with arbitrary shape, and its existence will affect the performance of the antenna or array and degrades the quality or property of electronic systems inevitably. For a number of years extensive research has been conducted on radome-antenna system and efficient analysis techniques [1-5] had also been developed for the accurate prediction of the behavior of electromagnetic (EM) performance. Due to the geometrical complexity of the radome-antenna system, its analysis is usually based on some approximate approaches [6-11], such as the methods based on the high-frequency approximation [6], integral equation models solved by the method of moments [7], the finite difference time domain (FDTD) method combined with the reciprocity theorem [8], and 3-D ray-tracing in conjunction with aperture integration method [9], coupled surface integral equation (CSIE) [10] and various fast solvers like the multilevel fast multi-pole algorithm (MLFMA) [11]. A hybrid physical optics method of moments (PO-MoM) scheme was also proposed to solve very large antenna-radome systems with sharp tip regions [12]. These analysis methods for the antenna-radome system are concentrated on the aspect that the antenna is placed in the interior of the dielectric radome. However, limited interior space of dielectric radome can't accommodate all electric systems, especially the large size antenna array, and the strong reciprocal interference between many radiation sources degrades the working quality of electronic systems, thus the model that the antenna is placed on the exterior of the dielectric radome is desirable, and it is also meaning to research on the performance of radome-antenna system in this layout.

Through our former working in [13] had involved the research on the end-fire antenna-radome system, the working was not refer to the physical behavior of dielectric radome and research the effect of dielectric radome on end-fire antenna with different polarization. Therefore, the objective of this paper is to investigate the effect of dielectric radome on radiation characteristics of conformal end-fire antenna mounted on a large conducting cylinder. A parametric study showing the impact of various parameters of dielectric radome on the antenna performance is presented. The simulation and analysis for the complete model are performed using the commercial computer software package Ansoft high-frequency structure simulator (HFSS), which is based on the finite element method.

II. EFFECT OF PLANAR DIELECTRIC LAYER ON THE INCIDENT PLANAR WAVE

In order to take insight into the physical behavior of dielectric radome and for simplicity, the section only

Submitted On: December 27, 2014
Accepted On: June 17, 2016

considers the physical mechanism when a planar wave is incident on a planar dielectric layer and dielectric constant ε_2 of dielectric layer is chosen to be same as dielectric radome ($\varepsilon_2 = \varepsilon_r = 5.5$, $\varepsilon_1 = \varepsilon_3 = 1$), as shown in Fig. 1. If amplitude of the incident planar wave is one, a transmitted field with a value of $T_{12}T_{23}$ in area 3 is produced when the plane wave is incident on two interfaces. However, the incident wave also produces second reflection in the material interface between dielectric layer and area 3, and creates second transmitted field with amplitude of $T_{12}R_{23}R_{21}T_{23}$. Similarly, second incident wave also produces third reflection in the material interface between dielectric layer and area 3, where T_{12} and T_{23} denote the transmission coefficient, R_{12} and R_{23} denote the reflection coefficient on two material interfaces. This shows that when a uniform plane wave is incident on lossless material interfaces with an angle of α, the total transmitted field in area 3 is the superposition of all transmitted fields, where *d* is the thickness of dielectric layer, β is the angle of refraction, and θ is the angle between transmission field and *z*-axis. Suppose that the coordinates of incidence point are (0, *d*), and the incident field is denoted as $E^i(0, d)$, and the transmission distance of refracted electromagnetic wave is represented as *P* in dielectric layer. Thus, when the planar wave is transmitted from the point (0, *d*) to the distance *r* away from the origin of the coordinate system, the variation of phase is the quantity $k_2P+k_3(r-P\sin\beta\sin\theta)$, where k_2 and k_3 are the propagation constants of electromagnetic wave in dielectric and vacuum, respectively.

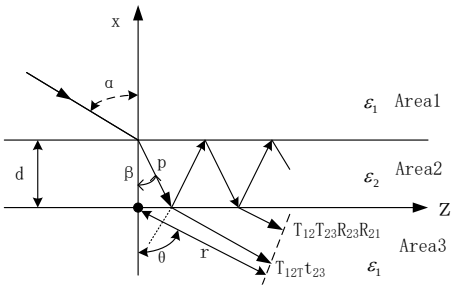

Fig. 1. EM wave is reflected and refracted many times in planar dielectric layer.

For simplicity, by setting $\Phi = k_2P - k_3P\sin\beta\sin\theta$, the phase of the first transmitted electromagnetic wave coming from a plane far away from the origin of the coordinate system with distance *r* can be expressed as $\Phi + k_3r$, the phase of the second transmitted electromagnetic wave coming from the same plane can be denoted as $3\Phi + k_3r$. Simultaneously, when it adds a reflection in the interior of substrate, the phase also adds a value of 2Φ . Therefore, the total field in area 3 can be denoted as:

$$\begin{aligned} E_{13} &= E^i(0,d)T_{12}T_{23}e^{(-j\Phi - jk_3r)}\left(1 + R_{21}R_{23}e^{-j2\Phi}\right. \\ &\quad \left. +(R_{21}R_{23})^2e^{-j4\Phi} + (R_{21}R_{23})^3e^{-j6\Phi} + ...\right) \qquad (1) \\ &= E^i(0,d)T_{12}T_{23}e^{(-j\Phi - jk_3r)}\frac{1}{1 - R_{21}R_{23}e^{-j2\Phi}}. \end{aligned}$$

From Eq. (1), it can be seen that the total field is interrelated with the transmission coefficient and the reflection coefficient on two material interfaces. Setting the transmission coefficient of E-field as:

$$T_e = \frac{T_{12}T_{23}}{1 - R_{21}R_{23}e^{-j2\Phi}}, \qquad (2)$$

where $\Phi = k_2P - k_3P\sin\beta\sin\theta = k_0d\sqrt{\varepsilon_2 - \varepsilon_1\sin^2\alpha}$.

Thus, the total E-field in area 3 can be expressed as;

$$E_{13} = E^i(0,d)T_e\exp(-j\Phi - jk_3r). \qquad (3)$$

On the other hand, according to the different directions of electric field vector, the incident plane wave can be divided into two different polarization types:

(1) TE Wave: the electric field vector is normal to the incident plane.

We assume that the dielectric layer is parallel to the *yz*-plane, and is normal to the *x*-axis, so the direction of *y*-axis is that of E-field. The reflection coefficient of electric field can be given by [14]:

$$R_E^{TE} = \frac{\cos\alpha - \sqrt{\frac{\varepsilon_2\mu_1}{\varepsilon_1\mu_2}}\sqrt{1 - \frac{\varepsilon_1\mu_1}{\varepsilon_2\mu_2}\sin^2\alpha}}{\cos\alpha + \sqrt{\frac{\varepsilon_2\mu_1}{\varepsilon_1\mu_2}}\sqrt{1 - \frac{\varepsilon_1\mu_1}{\varepsilon_2\mu_2}\sin^2\alpha}}. \qquad (4)$$

The transmission coefficient of electric field can be expressed as:

$$T_E^{TE} = 1 + R_E^{TE}, \qquad (5)$$

and the reflection coefficient of magnetic field also can be written as $R_H^{TE} = R_E^{TE}$, the transmission coefficient of magnetic field is $T_H^{TE} = \eta_1/\eta_2 \times T_E^{TE}$, where $\eta_1 = \sqrt{\mu_1/\varepsilon_1}$ and $\eta_2 = \sqrt{\mu_2/\varepsilon_2}$ are the wave impedances of electromagnetic wave in medium and vacuum, respectively.

(2) TM Wave: the electric field vector is parallel to the incident plane.

According to the Ref. [14], the reflection coefficient of magnetic field will be:

$$R_H^{TM} = \frac{\cos\alpha - \sqrt{\frac{\varepsilon_1\mu_2}{\varepsilon_2\mu_1}}\sqrt{1 - \frac{\varepsilon_1\mu_1}{\varepsilon_2\mu_2}\sin^2\alpha}}{\cos\alpha + \sqrt{\frac{\varepsilon_1\mu_2}{\varepsilon_2\mu_1}}\sqrt{1 - \frac{\varepsilon_1\mu_1}{\varepsilon_2\mu_2}\sin^2\alpha}}. \qquad (6)$$

The transmission coefficient of magnetic field can be expressed as $T_H^{TM} = 1 + R_H^{TM}$, and the reflection coefficient of electric field will be $R_E^{TM} = R_H^{TM}$ and the

transmission coefficient of electric field can be written as:

$$T_E^{TM} = \eta_2/\eta_1 \times T_H^{TM},$$

where $\eta_1 = \sqrt{\mu_1/\varepsilon_1}$ and $\eta_2 = \sqrt{\mu_2/\varepsilon_2}$ are the wave impedances of electromagnetic wave in medium and vacuum, respectively. Thus, it is clear from Eq. (3) that the power transmission coefficient $|T_e|^2$ can be calculated by using the transmission coefficient, the reflection coefficient and the value of Φ in any material interface as shown in Fig. 2.

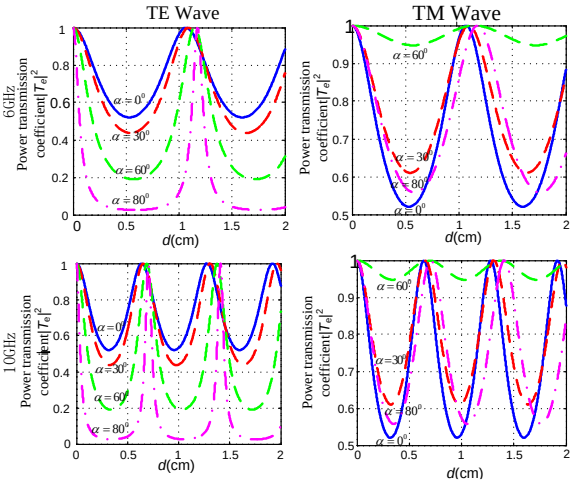

Fig. 2. Power transmission coefficient $|T_e|^2$ as a function of α, d and f.

It is obvious from Fig. 2 that when the thickness d of dielectric layer is close to zero and other parameters are chosen arbitrarily, the power transmission coefficient $|T_e|^2$ is close to one, which shows that the radome can be processed as thin dielectric layer by using unyielding dielectric to achieve higher transmission coefficient. It is also observed that for same incidence angle α the power transmission coefficient $|T_e|^2$ vary periodically with the thickness d of dielectric layer, and when the thickness d reaches a specific value the power transmission coefficient is close to one. As depicted in Fig. 1, choosing the phase difference between the two transmitted waves as $2\Phi = 2n\pi$, all transmitted waves will be superposed with same phase and the power transmission coefficient will reach its largest value. Thus the condition of achieving largest power transmission coefficient can be written as:

$$\Phi = k_0 d\sqrt{\varepsilon_2 - \varepsilon_1 \sin^2\alpha} = n\pi. \quad (7)$$

That is,

$$d = \frac{n\lambda}{2\sqrt{\varepsilon_2 - \varepsilon_1 \sin^2\alpha}}, \quad n=1,2,3,... \quad (8)$$

This shows that the power transmission coefficient has largest value when the thickness d of dielectric layer is selected by using Eq. (8).

III. EFFECT OF DIELECTRIC RADOME ON THE HORIZONTALLY POLARIZED ANTENNA

In this section, effect of dielectric radome on the horizontally polarized antenna based on balanced Vivaldi antenna (BAVA) is presented. The design of BAVA follows concepts described in [15], and it is designed to operate over 6–18 GHz frequency ranges. The proposed radome-antenna system is shown in Fig. 3. The antenna element is supported by using three dielectric cylinders, with height of h and dielectric constant 2.1, and is placed over a conducting cylinder surface of limited radius r=10 cm and length 15 cm. One end of three metal cylinder probes with radius of 0.6 mm is loaded by larger radius cylinder with thickness of 1 mm, whereas the other end firstly passes through dielectric cylinders with radius of 1.2 mm, and then is connected with the conducting cylinder surface, as shown in Fig. 3. The antenna surface is curved and is parallel to the cylinder surface, and the top edge of the antenna is parallel to the top edge of the conducting cylinder. A dielectric radome (dielectric constant $\varepsilon_r = 5.5$), whose generatrix is parabola curve and specifies in length P of 30 cm and thickness d of 5 mm, is presented. The generatrix equation can be expressed as:

$$\begin{aligned} x_o &= -az_0^{\,n} + r, \\ x_i &= -a_1 z_i^{\,n} + r - d, \end{aligned} \quad (9)$$

where a=r/P^n, a_1=(r-d)/(P-d)^n, n denotes the power index, x_0 is the distance between exterior generatrix and center line, z_0 is the variable value in z-direction, x_i is the distance between interior generatrix and center line, z_i is the variable value in z-direction.

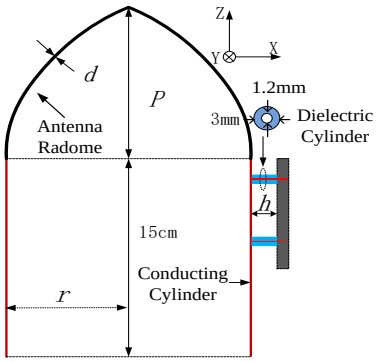

Fig. 3. Radome-antenna system based on balanced Vivaldi antenna.

Figure 4 shows the comparison of the radiation

patterns with two examples, i.e., without antenna radome and with antenna radome for both E_Φ and E_θ. It is seen clearly that when no antenna radome is used, the main beam of the antenna is directed to the end-fire direction and the antenna has low cross polarization of less than -20 dB. When the dielectric radome is placed on the top part of conducting cylinder, the electromagnetic wave from radiator will be reflected and refracted by the dielectric surface, which leads to the large beam direction angle in H-plane, such as at 6 GHz, beam direction angle is 27^0 and the 3 dB beam-width is 57^0 without dielectric radome, whereas the beam direction angle and 3 dB beam-width are 30^0 and 35^0 respectively with dielectric radome; at 12 GHz, beam direction angle is 0^0 and the 3 dB beam-width is 48^0 without dielectric radome, whereas the beam direction angle and 3 dB beam-width with dielectric radome become 130^0 and 100^0, respectively. The measured radiation pattern without dielectric radome also is presented to compare with simulated results, which shows that the simulation and measurement results generally agree, however a little discrepancy has been observed possibly due to the error of substrate parameters and manufacturing tolerances. Figure 5 shows the simulated E-field in H-plane (xz-plane), which demonstrates the impact of the dielectric radome on E-field. It is clearly seen from the figure that when an antenna radome is placed on the top part of conducting cylinder, for the low frequency the main energy is reflected by the surface of dielectric radome, whereas as the frequency is increased to 12 GHz a part of energy is transmitted through antenna radome. This is due to the fact that at 12 GHz the wavelength in air is 25 mm, but will be around 10.7 mm in material with dielectric constant ε_r=5.5, so the thickness of antenna radome is close to half-wavelength in dielectric. As a result, reflection coefficients in internal and external surfaces of dielectric radome have converse symbols, which lead to larger transmission coefficient.

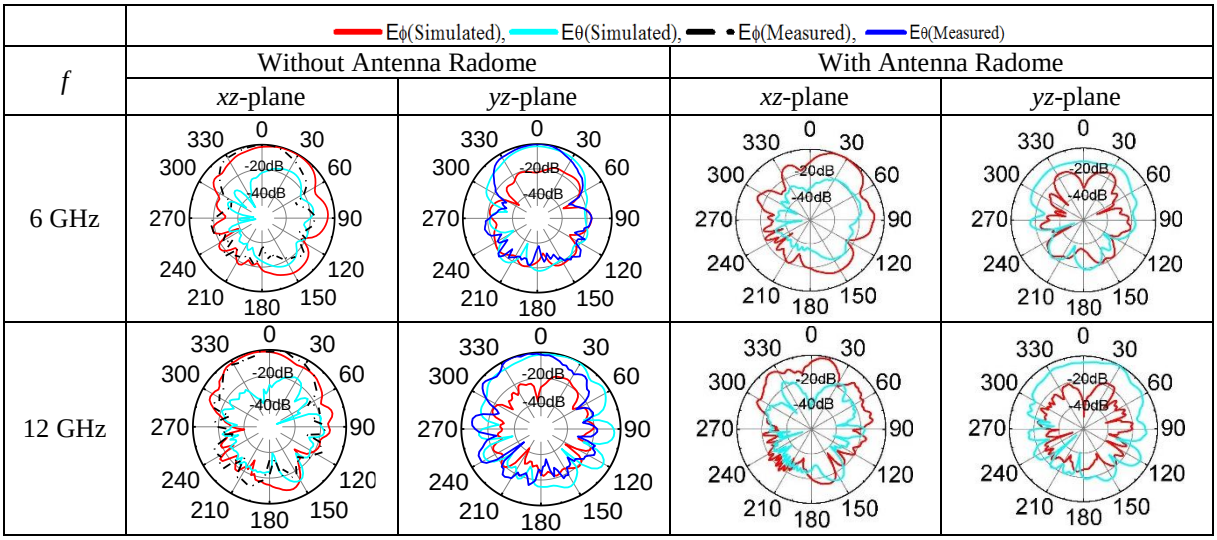

Fig. 4. Comparison of radiation pattern of the horizontal polarization antenna.

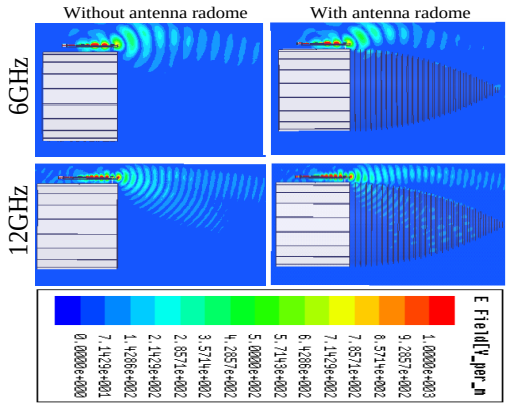

Fig. 5. Comparison of simulated radiated E-field of the horizontal polarization antenna in H-plane.

IV. EFFECT OF DIELECTRIC RADOME ON THE VERTICALLY POLARIZED ANTENNA

In order to meet the bandwidth requirement of 6-18 GHz a cascaded monopole log-periodic antenna configuration is selected, as shown in Fig. 6. The proposed antenna has a single-layer metallic structure and is printed on a substrate of thickness 0.724 mm, with the dielectric constant of 3.38, and is located above the metal conducting cylinder surface vertically. A 50 Ω coaxial cable is used as the feed source, whose outer conductor is directly soldered to metal ground plane, whereas the inner conductor is connected directly to the one end of cascaded folded microstrip-line, and other end is shorted to the ground plane for reducing the end reflection. As shown in Fig. 6, the geometry is specified by the following parameters: the height of the folded

microstrip-line P_1, the gap G_1, the vertically strip width and horizontally strip width in arm of first folded pairs w_1 and wf_1, and the transmission strip width s_1, the strip spacing in arm a_1, the transmission strip length b_1, and the scaling factor τ. All these parameters are decreased along the array by the scaling factor τ, which are expressed as:

$$\tau = \frac{P_2}{P_1} = \frac{w_2}{w_1} = \frac{a_2}{a_1} = \frac{wf_2}{wf_1} = \frac{b_2}{b_1} = \frac{G_2}{G_1} = \frac{s_2}{s_1}. \quad (10)$$

The length $(2P_1+a_1)$ of first folded microstrip-line is approximately half-wavelength at a frequency which is referred to as the lowest working frequency. The dielectric top edge of the proposed antenna is parallel to the top edge of conducting cylinder. Simulation and analysis of the radome-antenna system are performed using the package ANSYS high-frequency structure simulator (HFSS), and the optimized values are illustrated in Table 1.

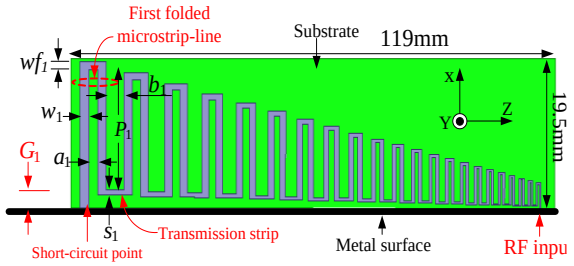

Fig. 6. Configuration of the proposed vertically polarized antenna.

Table 1: Parameters of the proposed antenna as Fig. 6

Parameter	P_1	G_1	w_1	wf_1
Values	12.5 mm	1 mm	4.76 mm	4.76 mm
Parameter	a_1	b_1	s_1	τ
Values	1.96 mm	1.76 mm	2.5 mm	0.88

Figure 7 shows the radome-antenna system based on cascaded monopole log-periodic antenna, which is same as the model presented in Fig. 3. It may also be mentioned that due to the radiated E-filed is vertical to the metal surface of conducting cylinder, thus the radiant electromagnetic wave of cascaded monopole log-periodic antenna can be approximated to the TM wave, and exhibits similar variations trend which has been presented in the theory analysis in Section II. Figure 8 only shows the radiation pattern of the vertically polarized antenna at two most influential frequencies. For other working frequencies, it is known from simulation that the dielectric radome has smaller effect on the radiation patterns of the vertically polarized antenna comparing to that of the horizontally polarized antenna, which is not presented in this paper owing to limited space. It is clearly seen from Fig. 8 that at 8 GHz the effect of the dielectric radome is very serious, which is due to the fact that as the frequency is increased, the effective radiation area is close to the top edge of conducting cylinder, the incidence angle of the radiant electromagnetic wave incident on the surface of dielectric radome becomes smaller (such as about 60^0). According to the theory of Section II, the power transmission coefficient also becomes larger, thus a radiated blind area will be appeared in end-fire direction. When the frequency is increased continuously which means that the incidence angle also becomes smaller, such as increasing to 12 GHz, but the radiation pattern is also subjected to the significant effect of the dielectric radome owing to the dielectric radome resonance.

Figure 9 shows the simulated radiated E-field in E-plane (xz-plane). It should be observed that without dielectric radome introduced, at low frequency the dominant currents are covered in whole folded metal microstrip-line, the metal surface has little influence on the radiation pattern, resulting in a main beam directed in the end-fire direction. When the antenna is worked in higher frequency range the resonant dominant currents are concentrated in the close proximity of the feed port, the main beam only is deviated from the end-fire direction slightly. However, due to the presence of the nearby dielectric radome, the radiated electromagnetic waves from the proposed antenna are significantly affected. It is also observed that a part of energy is transmitted through dielectric radome and deviated from its original radiant direction owing to refraction phenomena, which shows the similar behavior with horizontally polarized antenna.

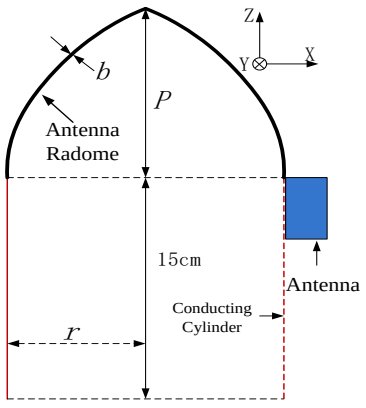

Fig. 7. Radome-antenna system based on cascaded monopole log-periodic antenna.

f	Without Antenna Radome		With Antenna Radome	
	xz-plane	*yz*-plane	*xz*-plane	*yz*-plane
8 GHz	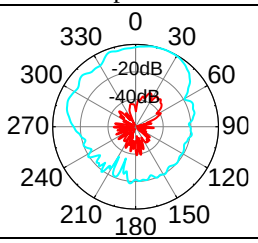	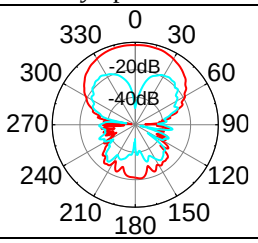	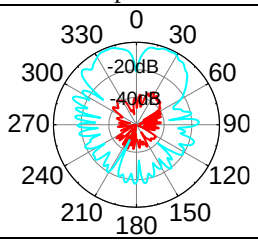	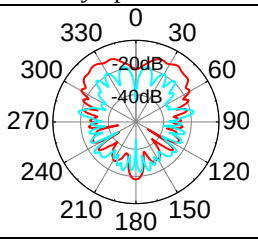
12 GHz	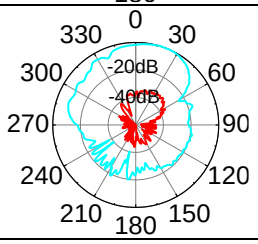	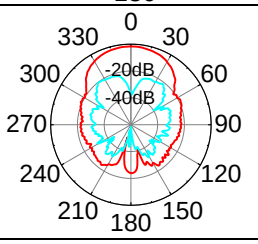	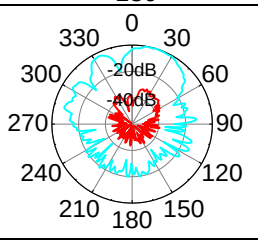	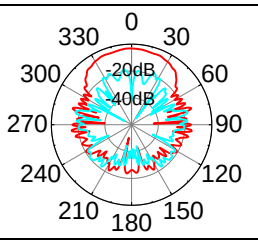

Fig. 8. Comparison of radiation pattern of the vertical polarization antenna. (— Eϕ; — Eθ)

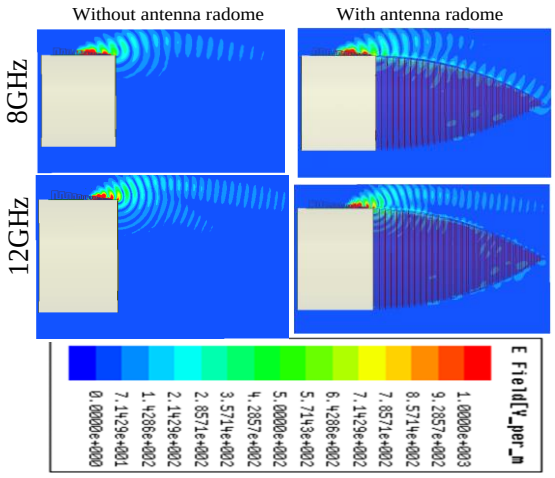

Fig. 9. Comparison of simulated radiated E-field of the vertical polarization antenna in E-plane.

V. PARAMETRIC STUDIES

In Section III and IV, a comparison of the effect of the dielectric radome on different polarization types is studied, which shows that the affect of dielectric radome on vertically polarized endfire antenna is less than that on the horizontally polarized endfire antenna, thus the vertically polarized endfire antenna is suitable for the proposed model. In this section, parametric studies about dielectric radome based on the cascaded monopole log-periodic antenna are presented. The parameters under study include the bottom plane radius r, height P, thickness b, power index n, and dielectric constant ε_r. To better understand the influence of the parameters on the radiation pattern, only one parameter at a time will be varied, while others are kept unchanged unless especially indicated.

A. Bottom plane radius *r* of dielectric radome

Figure 10 shows the effect of variation of the bottom plane radius r on the radiation pattern. It is obvious from the figure that in E-plane (*xz*-plane) the variation of radius r has little effect on the radiation pattern and the radiation pattern keeps low cross-polarization levels (<-30 dB). In H-plane (*yz*-plane) as the radius r is increased the front-back ratio of the antenna is also enhanced slightly. In the cross-polarization curves, the cross-polarization level is decreased by increasing radius r. This is due to the fact that smaller radius r of conducting cylinder will inspirit the higher mode, which leads to high cross-polarization levels.

B. Height *P* of dielectric radome

Figure 11 demonstrates the impact of varying the height P on the radiation pattern of the vertical polarization antenna. The figure shows that in E-plane (*xz*-plane) with increasing the height P from 10 to 30 cm, the antenna keeps low cross-polarization levels (<-30 dB), and the co-polarization curves almost keep invariable at working frequency, but in the co-polarization curve a deep blind area has been appeared in end-fire direction. In H-plane (*yz*-plane), the cross-polarization level becomes larger and the largest value varies around -20 dB. Moreover, the front-back ratio of the co-polarization curves is also increased slightly as the height P is increased. This is due to the fact that when the height P=30 cm, more energy is incident on the surface of dielectric radome, and the dielectric radome can enhance the directive function of the radiation field shown in Fig. 9. Results from the figure have revealed that in order to achieve a good radiation pattern a small height P needs

be adopted properly.

C. Thickness *b* of dielectric radome

The effect of varying the thickness *b* of dielectric radome on the radiation pattern is presented in Fig. 12. It is clearly seen from the figure that in E-plane (*xz*-plane) when the thickness *b* is decreased, the antenna keeps low cross-polarization levels, and shows better co-polarization curves. It may be noted that with increasing the thickness b, the dielectric radome resonance is pulled to the lower frequency band, thus the blind area will be appeared in co-polarization curves at lower frequency band. In H-plane (*yz*-plane), the variation of thickness *b* has significant effect on the cross- and co-polarization levels. As the thickness *b* is increased the cross-polarization levels become worse, whereas the cross-polarization levels in the end-fire direction is decreased slightly, generally less than -40 dB. For co-polarization curves, increasing thickness *b* will lead to higher front-back ratio. However, the radiation pattern is still almost symmetric with respect to the *z*-axis in *yz*-plane. It is also observed from the figure that smaller dielectric thickness *b* will produce smoother co-polarization curve. Thus, the antenna has good performance when the dielectric radome keeps small thickness *b*.

D. Power index *n* of the generatrix equation

Figure 13 shows the effect of varying the power index *n* on the radiation pattern. The results show that the variation of power index *n* has significant effect on the cross- and co-polarization levels. In E-plane (*xz*-plane), with increasing power index *n* the antenna also keeps low cross-polarization level, generally less than -30 dB. When the antenna is working in low frequency, the variation of power index *n* has little effect on the radiation pattern, but in high frequency as the power index *n* is increased, the co-polarization curve produces large variation and blind area of co-polarization curves becomes deeper. In H-plane (*yz*-plane), the cross-polarization levels, generally less than -30 dB. However, the co-polarization curve produces large variation and blind area of co-polarization curves becomes deeper as the power index *n* is increased. In H-plane (*yz*-plane), the cross-polarization level in end-fire direction is less than -40 dB, and has little variation as the index *n* is increased. However, the co-polarization curve in high frequency has large variation, and the front-back ratio is increased slightly with decreasing the power index *n*. Therefore, the antenna has good end-fire characteristics when the power index has smaller value.

E. Dielectric constant ε_r of dielectric radome

Figure 14 demonstrates the impact of varying dielectric constant ε_r on the radiation pattern. It is found that in E-plane (*xz*-plane) the variation of dielectric constant ε_r has little effect on the cross-polarization levels and the antenna also keeps low cross-polarization level, generally less than -30 dB. But the 3 dB beam-width of the co-polarization radiation field is decreased as the dielectric constant ε_r is increased, and the dielectric radome resonance is also produced in high frequency. This is also due to the fact that the thickness of dielectric radome is close to the half-wavelength when the antenna is working in higher frequency and leads to refraction phenomenon of a part of energy. In H-plane (*yz*-plane), the antenna also keeps low cross-polarization levels, and as the dielectric constant ε_r is increased the co-polarization curves still keep symmetric radiation pattern. It is obvious from the figure that smaller the dielectric constant ε_r better the radiation pattern will be.

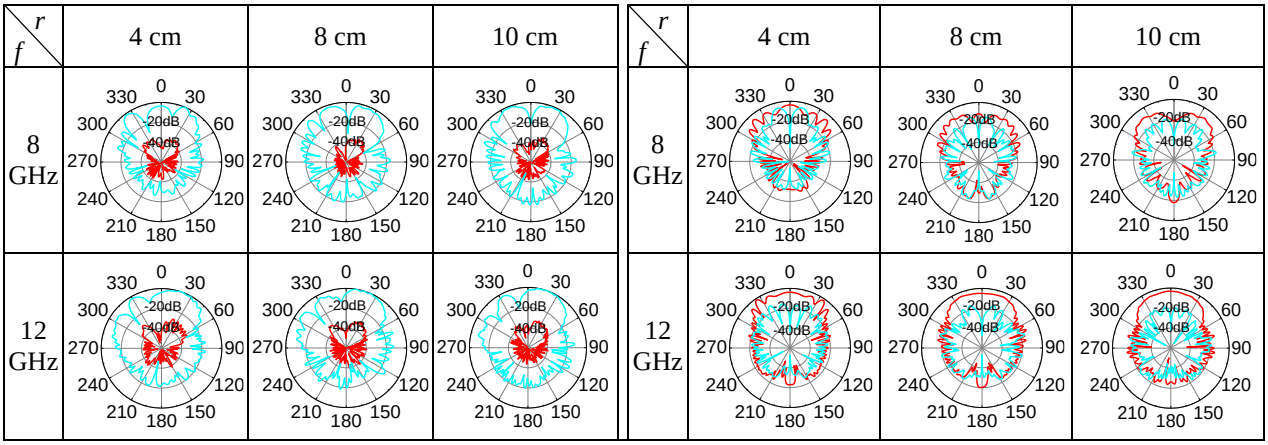

(a) *xz*-plane (b) *yz*-plane

Fig. 10. Effect of varying the bottom plane radius *r* on the radiation pattern. (— Eϕ; — Eθ)

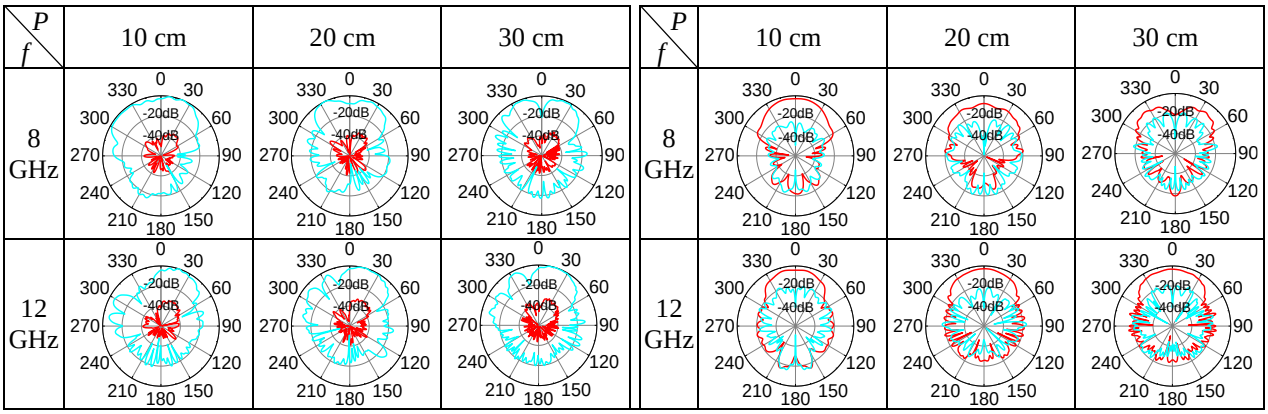

(a) *xz*-plane (b) *yz*-plane

Fig. 11. Effect of varying the height *P* on the radiation pattern. (— Eϕ; — Eθ)

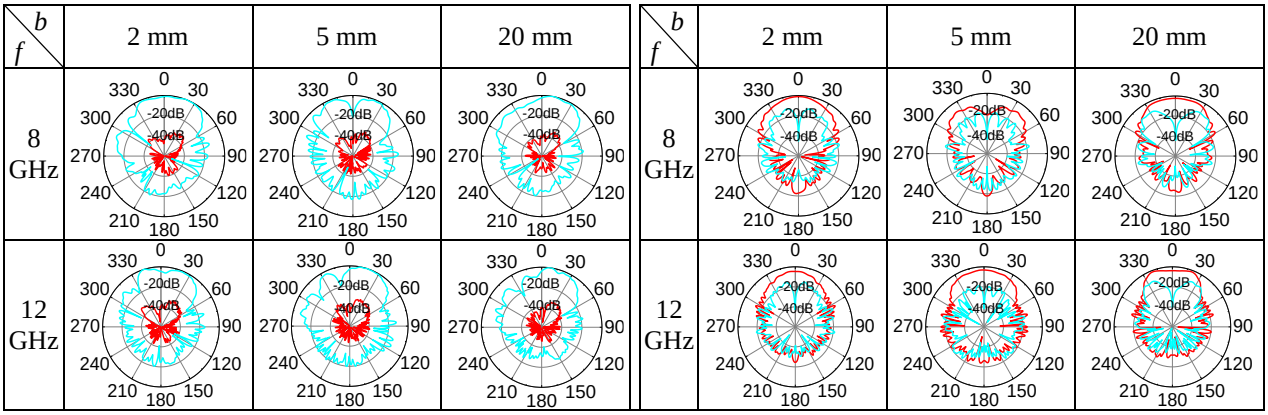

(a) *xz*-plane (b) *yz*-plane

Fig. 12. Effect of varying the thickness *b* on the radiation pattern. (— Eϕ; — Eθ)

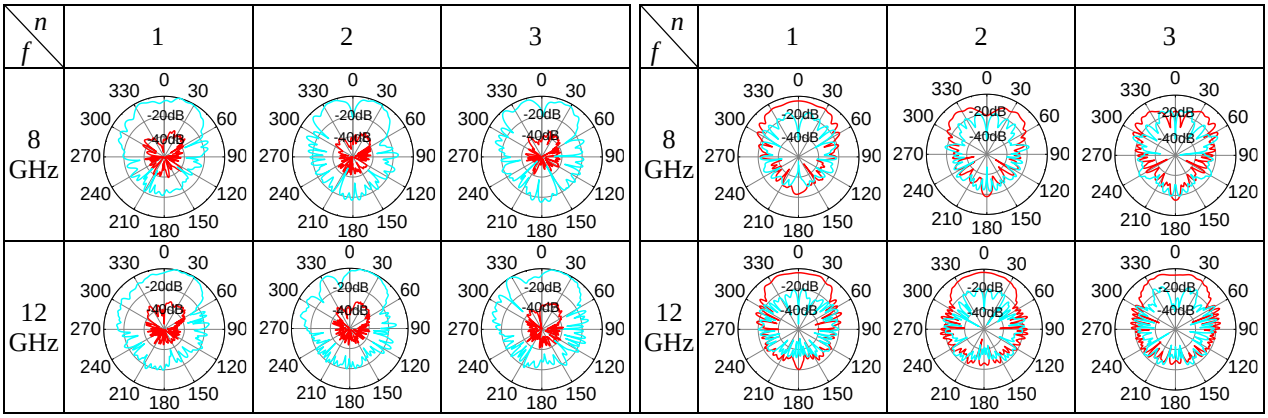

(a) *xz*-plane (b) *yz*-plane

Fig. 13. Effect of varying the power index *n* on the radiation pattern. (— Eϕ; — Eθ)

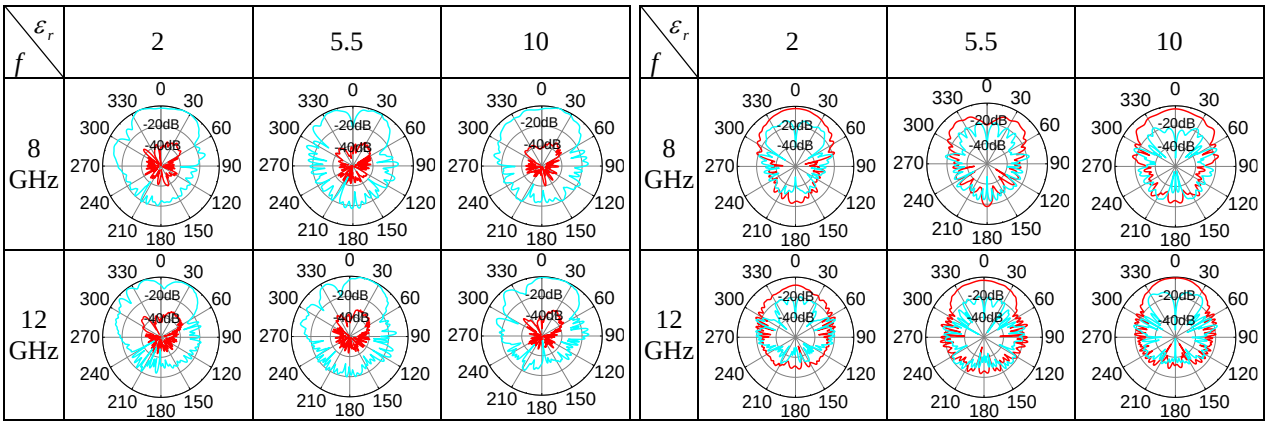

(a) *xz*-plane (b) *yz*-plane

Fig. 14. Effect of varying the dielectric constant ε_r on the radiation pattern. (— Eφ; — Eθ)

VI. CONCLUSION

In this paper, an analysis on the effect of dielectric radome on radiation field of conformal end-fire antenna mounted on a large conducting cylinder is presented. The paper firstly analyzes the effect of planar dielectric layer on the plane wave with different polarizations, and gives the expression for the transmitted electric field and the power transmission coefficient to show their relation with thickness of dielectric layer and incidence angle. Then, a comparison of the effect of the dielectric radome on conformal end-fire antennas with different polarizations is presented. It has been found that the effect of the dielectric radome on the radiation pattern of the vertically polarized endfire antenna is less than that on the horizontally polarized endfire antenna. Finally, the effect of a nearby dielectric radome on the vertically polarized antenna's radiation characteristics has been examined, which show that with use of a larger radius *r*, smaller height *P*, smaller thickness *b*, smaller power index *n* and dielectric constant ε_r, a better end-fire radiation pattern can be achieved. The investigation should be helpful to the design of radome-antenna system.

ACKNOWLEDGMENT

This work is supported by the Changjiang Scholars and Innovative Research Team in University under Grant No. IRT1299, and Doctoral fund of Chongqing University of Posts and Telecommunications (A2015-08).

REFERENCES

[1] D. C. F. Wu and R. C. Ruduck, "Plane wave spectrum-surface integration technique for radome analysis," *IEEE Trans. Antennas Propag*., vol. 22, no. 3, pp. 497-500, 1974.

[2] S. W. Lee, M. S. Sheshadri, V. Jamnejad, and R. Mittra, "Wave transmission through a spherical dielectric shell," *IEEE Trans. Antennas Propag*., vol. 30, no. 3, pp. 373-380, 1982.

[3] X. J. Gao and L. B. Felsen, "Complex ray analysis of beam transmission through two-dimensional radomes," *IEEE Trans. Antennas Propag.*, vol. 33, no. 9, pp. 963-975, 1985.

[4] R. Orta, R. Tascone, and R. Zich, "Performance degradation of dielectric radome covered antennas," *IEEE Trans. Antennas Propag.*, vol. 36, no. 12, pp. 1707-1713, 1988.

[5] D. J. Kozakoff, *Analysis of Radome-Enclosed Antennas*. Norwood, MA: Artech House, 1997.

[6] X. J. Gao and L. B. Felsen, "Complex ray analysis of beam transmission through two-dimensional radomes," *IEEE Trans. Antennas Propag.*, vol. 33, no. 9, pp. 963-975, 1985.

[7] H. Mustacoglu, J. R. Mautz, and E. Arvas, "MoM analysis of an axisymmetric chiral radome," *Appl. Comp. Electromagnetics Society (ACES) Journal*, vol. 28, no. 3, Mar. 2013.

[8] B. Lin, S. Du, H. Zhang, and X. Ye, "Design and simulation of frequency-selective radome together with a monopole antenna," *Appl. Comp. Electro-magnetics Society (ACES) Journal*, vol. 25, no. 7, pp. 620-625, July 2010.

[9] R. U. Nair and R. M. Jha, "Electromagnetic performance analysis of a novel monolithic radome for airborne applications," *IEEE Trans. Antennas Propag.*, vol. 57, no. 11, pp. 3664-3668, 2009.

[10] M. He, "On the characteristics of radome enclosed archimedean spiral antennas," *IEEE Trans. Antennas Propag.*, vol. 56, no. 7, pp. 1867-1874, 2008.

[11] C. C. Lu, "A fast algorithm based on volume integral equation for analysis of arbitrarily shaped dielectric radomes," *IEEE Trans. Antennas Propag.*, vol. 51, no. 3, pp. 606-612, 2003.

[12] M. A. A. Moneum, Z. Shen, J. L. Volarjis, and O. Graham, "Hybrid PO-MoM analysis of large axi-symmetric radomes," *IEEE Trans. Antennas Propag.*, vol. 49, no. 12, pp. 1657-1665, 2001.

[13] P. Wang, G. J. Wen, H. B. Zhang, and Y. H. Sun, "A wideband conformal end-fire antenna array mounted on a large conducting cylinder," *IEEE Trans. Antennas Propag.*, vol. 61, no. 9, pp. 4857-4861, 2013.

[14] K. Q. Zhang and D. J. Li, *Electromagnetic Theory in Microwave and Optoelectronics*. Publishing House of Electronic Industry, China, 2001.

[15] J. D. S. Langley, P. S. Hall, and P. Newham, "Balanced antipodal vivaldi antenna for wide bandwidth phased arrays," *IEE Proc Microw. Antenna Propag.*, vol. 143, no. 2, pp. 97-102, 1996.

Ping Wang was born in Chongqing, China. He received his M.S. degree in Theoretical Physics from Chongqing University of China in 2008 and the Ph.D. degree in University of Electronic Science and Technology of China (UESTC) in 2013, respectively. Currently, he is working in Chongqing University of Posts and Telecommunications, China. His current research interests include patch antennas, wideband antennas, and arrays.